Charm Production at Low Q^2 With the ZEUS Detector

Gayane Aghuzumtsyan (on behalf of the ZEUS Collaboration)

Physikalisches Institut, University of Bonn

Abstract. The production of $D^*(2010)$ mesons in deep inelastic scattering at low Q^2 has been measured with the ZEUS detector at HERA using an integrated luminosity of 81.9 pb^{-1}. The D^* mesons have been reconstructed from their decay into D^0 and π_s with the decay $D^0 \to K^-\pi^+$ and corresponding antiparticle decay. Differential D^* cross sections as functions of exchanged photon virtuality, Q^2, inelasticity, y, transverse momentum of the D^* meson, $p_T(D^*)$, and pseudorapidity of the D^* meson, $\eta(D^*)$, have been measured, using the beam-pipe calorimeter of ZEUS. The kinematic region of the measurement is $0.05 < Q^2 < 0.7$ GeV^2, $0.02 < y < 0.85$, $1.5 < p_T(D^*) < 9.0$ GeV and $|\eta(D^*)| < 1.5$. The measured differential cross sections are compared with the predictions of next-to-leading-order QCD.

Keywords: Charm, production, D*, low Q^2, cross sections, QCD
PACS: 12.38.Bx, 12.38.Qk, 13.25.Ft, 13.60.Le, 13.85.Hd, 14.40.Lb

INTRODUCTION

Charm quarks have been measured both in photoproduction and in deep inelastic scattering (DIS) at HERA [1, 2, 3, 4, 5]. The measurements are reasonably described by perturbative QCD calculations where the charm is produced mainly by boson-gluon fusion (BGF).

Charm production in the transition region from DIS to photoproduction is probed. Event containing D^* mesons were selected in which the virtuality of the exchanged photon , Q^2, lies in the range $0.05 < Q^2 < 0.7$ GeV^2. The measurement was performed using the beam pipe calorimeter (BPC) [6, 7]. Differential D^* cross sections have been measured as a function of Q^2, y, $p_T(D^*)$ ans $\eta(D^*)$ and compared to NLO predictions using the HVQDIS program.

EVENT SELECTION AND DATA ANALYSIS

The data from the years 1998-2000 with an integrated luminosity of 82 pb^{-1} have been analysed with the ZEUS [8] detector at HERA, where protons of energy E_p = 920 GeV collided with the electrons or positrons of energy E_e = 27.5 GeV.

Events which fulfil the following conditions were selected: characteristic energy deposit of an electron within the fiducial area of the BPC with $E_{\text{BPC}} > 4$ GeV; BPC timing measurement consistent with an ep interaction $| < \tau_{\text{BPC}} > | < 3$ ms; a primary vertex with $|Z_{\text{vertex}}| < 50$ cm was reconstructed; the ratio of the transverse momentum of the D^* to the total tranverse CAL energy deposit was $p_T(D^*)/E_T > 0.1$ and $35 < \delta_{\text{BPC}} < 65$ GeV, where $\delta_{\text{BPC}} = \delta + E_{\text{BPC}}(1 - \cos(\Theta_{\text{BPC}}))$, $\delta = \sum_i (E - p_z)_i$, the index i runs over the CAL clusters, and $\Theta_{\rm BPC}$ is the angle of the scattered electron w.r.t. the proton beam axis. Events with an additional reconstructed electron in the calorimeter are suppressed.

The selected kinematic region was $0.05 < Q^2 < 0.7$ GeV^2 and $0.02 < y < 0.85$.

D^* mesons were reconstructed from tracks in the decay channel $D^{*+} \to D^0 \pi_s^+$ (+c.c.) with $D^0 \to K^- \pi^+$ (+c.c.). Pairs of well-reconstructed tracks with $p_T > 0.45$ GeV were combined to form a D^0 candidate. A third track with $p_T > 0.12$ GeV and charge opposite to that of the kaon track was combined with the D^0 candidate to form a D^* candidate, and kept if its charge was opposite to the kaon track. A different mass window for the D^0 was used for each bin of $p_T(D^*)$ from $1.82 < M(K\pi) < 1.91$ GeV, to $1.79 < M(K\pi) < 1.94$ GeV. To allow the background to be determined, D^0 candidates with wrong-sign combinations, in which both tracks forming the D^0 candidates have the same charge and third track has the opposite charge, were also retained.

D^* mesons were selected in the kinematic region $1.5 < p_T(D^*) < 9$ GeV and $|\eta(D^*)| < 1.5$.

Figure 1 shows the distribution of $\Delta M = M(D^*) - M(D^0)$ for the reconstructed events. A clear signal is seen around the nominal value of ΔM. The number of D^* mesons, extracted by an unbinned fit, was $N(D^*) = 253 \pm 25$.

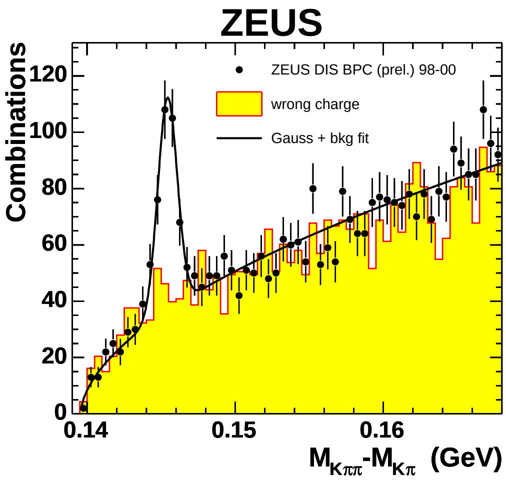

FIGURE 1. The distribution of the mass difference, $\Delta M = M(K\pi\pi_s) - M(K\pi)$, for $D^{*\pm}$ candidates from BPC measurements. The histogram shows the ΔM distribution for wrong charge combinations. The solid curve represents the fi t.

CROSS SECTIONS

The inclusive D^* cross sections at low Q^2 were measured in the kinematic region $0.05 < Q^2 < 0.7$ GeV^2, $0.02 < y < 0.85$, $1.5 < p_T(D^*) < 9$ GeV and $|\eta(D^*)| < 1.5$. The HERWIG [9] Monte Carlo program was used to correct the data for detector effects and calculate acceptances. The measured cross section is

$$\sigma(e^{\pm} p \to e^{\pm} D^* X) = 10.1 \pm 1.0 \text{ (stat) } {}^{+1.1}_{-0.8} \text{(syst) nb.} \quad (1)$$

The replacement of HERWIG by RAPGAP [10] for acceptance corrections was the main source of systematic error (8%).

The NLO prediction of the $c\bar{c}$ cross section was obtained using the program HVQDIS. The fragmentation of the charm quarks was performed according to the Peterson model with the parameter $\varepsilon = 0.035$. The nominal mass of the charm quark was set to $m_c = 1.35$ GeV. The normalisation and factorisation scales were set to $\mu = \sqrt{Q^2 + 4m_c^2}$. The ZEUS NLO QCD fit and CTEQ5F3 were used as the parametrisation of the proton PDFs. The NLO predicted total cross section is

$$\sigma_{\mathrm{HVQDIS}}(e^{\pm}p \rightarrow e^{\pm}D^{*}X) = 8.6^{+1.9}_{-1.8}(\mathrm{syst.})\,\mathrm{nb} \tag{2}$$

To estimate the theoretical uncertainty, the ZEUS PDF fit was used and the scale μ, the mass of the charm quark and the parameter ε in the Peterson fragmentation function were varied in the range: $(Q^2 + m_c^2) < \mu^2 < 4(Q^2 + 4m_c^2)$, $1.2 < m_c < 1.5$ GeV, $0.02 < \varepsilon < 0.05$, respectively.

Figure 2 shows the single differential cross sections as a function of Q^2, y, $p_T(D^*)$ and $\eta(D^*)$ compared to the NLO QCD predictions. In general, shape and normalization of the distributions are described by the NLO predictions. A comparison of $d\sigma/dQ^2$ with previous ZEUS results is shown in figure 3. For this figure, in order to have data comparable to older measurements, the y range was restricted to $0.02 < y < 0.7$. The unbinned fit in this restricted kinematic region yielded $N(D^*) = 239 \pm 23$. The transition from high to low Q^2 is well described by the predictions, and therefore well understood.

SUMMARY

The production of D^* mesons in DIS at HERA was measured with the ZEUS detector in the kinematic region $0.05 < Q^2 < 0.7$ GeV^2, $0.02 < y < 0.85$, $1.5 < p_T(D^*) < 9$ GeV, $|\eta(D^*)| < 1.5$, probing the transition region to photoproduction regime. The theoretical NLO QCD calculation of BGF charm production is consistent with the measured cross sections at low Q^2. A comparison to data at higher Q^2 shows that this transition region is well understood.

REFERENCES

1. H1 Coll., C. Adolf et el. *Phys. Lett.*, **B 528**, 199 (2002).
2. ZEUS Coll., J. Breitweg et al., *Phys. Lett.*, **B 481**, 213 (2000).
3. ZEUS Coll., J. Breitweg et al., *Eur. Phys. J.*, **C 12**, 35 (2000).
4. H1 Coll., C. Adolf et el. *Nucl. Phys.*, **B 545**, 21 (1999).
5. ZEUS Coll., J. Breitweg et al., *Eur. Phys. J.*, **C 6**, 67 (1999).
6. C. Amelung, *Measurement of Proton Structure Function F_2 at Very Low Q^2 at HERA*, Ph.D. Thesis, Universität Bonn, Bonn, (Germany), Report BONN-IR-99-15, DESY-THESIS-2000-002,1999.
7. B. Surrow, *Measurement of the Proton Structure Function F2at Low Q^2 and Very Low x with the ZEUS Beam Pipe Calorimeter at HERA*, Ph.D. Thesis, University Hamburg, Hamburg, (Germany), DESY Report DESY-THESIS-1998-004.
8. ZEUS Coll., U. Holm et al.,*The ZEUS Detector*, DESY Status Report (unpublished), 1993, *www-zeus.desy.de/bluebook/bluebook.html*.
9. ZEUS Coll., G. Marchesini et al.,*Comp.Phys. Comm.*, **67**, 465 (1992).
10. H. Jung,*Comp. Phys. Commun.*, **86**, 147 (1995).

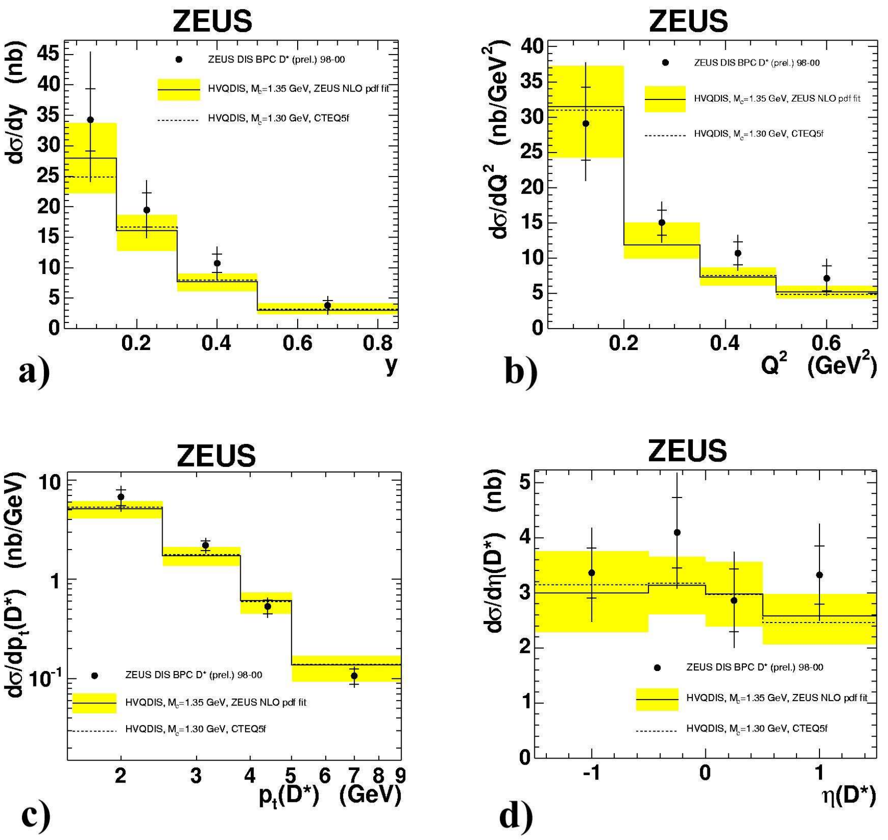

FIGURE 2. Differential D^* cross sections as a function of y (a), Q^2 (b), $p_T(D^*)$ (c) and $\eta(D^*)$ for low Q^2 compared to the NLO predictions from HVQDIS.

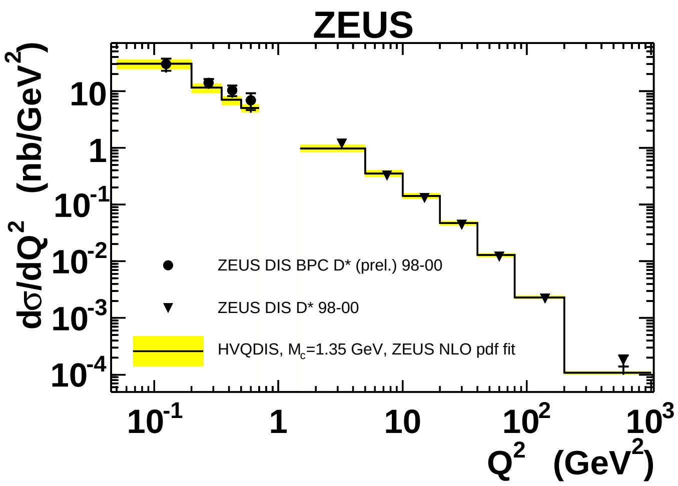

FIGURE 3. Differential D^* cross sections as a function of Q^2 for low Q^2 and from previous results on D^* production in DIS compared to the NLO predictions from HVQDIS.